Upregulation of P2X7 Exacerbates Myocardial Ischemia–Reperfusion Injury through Enhancing Inflammation and Apoptosis in Diabetic Mice

Fancan Wu,*,[1] Hong Wei,*,†,[1] Yingxin Hu,* Jiahong Gao,* and Shiyuan Xu*

Diabetes-aggravated myocardial ischemia–reperfusion (MI/R) injury remains an urgent medical issue, and the molecular mechanisms involved with diabetes and MI/R injury remain largely unknown. Previous studies have shown that inflammation and P2X7 signaling participate in the pathogenesis of the heart under individual conditions. It remains to be explored if P2X7 signaling is exacerbated or alleviated under double insults. We established a high-fat diet and streptozotocin-induced diabetic mouse model, and we compared the differences in immune cell infiltration and P2X7 expression between diabetic and nondiabetic mice after 24 h of reperfusion. The antagonist and agonist of P2X7 were administered before and after MI/R. Our study showed that the MI/R injury of diabetic mice was characterized by increased infarct area, impaired ventricular contractility, more apoptosis, aggravated immune cell infiltration, and overactive P2X7 signaling compared with nondiabetic mice. The major trigger of increased P2X7 was the MI/R-induced recruitment of monocytes and macrophages, and diabetes can be a synergistic factor in this process. Administration of P2X7 agonist eliminated the differences in MI/R injury between nondiabetic mice and diabetic mice. Both 2 wk of brilliant blue G injection before MI/R and acutely administered A438079 at the time of MI/R injury attenuated the role of diabetes in exacerbating MI/R injury, as evidenced by decreased infarct size, improved cardiac function, and inhibition of apoptosis. Additionally, brilliant blue G blockade decreased the heart rate after MI/R, which was accompanied by downregulation of tyrosine hydroxylase expression and nerve growth factor transcription. In conclusion, targeting P2X7 may be a promising strategy for reducing the risk of MI/R injury in diabetes. ***The Journal of Immunology*****, 2023, 210: 1962–1973.**

Cardiovascular events are the leading cause of death in patients with diabetes (1). Myocardial vulnerability of patients with diabetes depends on the progression and duration of diabetes (2). With the development of percutaneous coronary intervention, patients with myocardial infarction are effectively treated, but there is still a high mortality rate after reperfusion, which is as high as 7% in 1 y (3). Among them, patients with diabetes have higher restenosis and a lower long-term survival rate, which is associated with aggravated myocardial ischemia–reperfusion (MI/R) injury (4). The underlying mechanisms are complicated. Identification of mechanisms between diabetes and increased vulnerability to MI/R injury has medical value and may reveal promising targets for treating ischemic heart disease in patients with diabetes.

The P2X7 receptor belongs to the ligand-gated ion channel P2X subfamily of purine-based P2 receptors, and overactivation of P2X7 is involved in the progression of inflammation and cardiovascular disease (5). The most significant downstream effect of P2X7 activation is the nucleotide-binding oligomerization domain-like receptors family pyrin domain-containing 3 (NLRP3) inflammasome assembly and cleavages of pro-caspase-1 to caspase-1, resulting in the activation of pro-IL-1β into its mature form, which is the primary agent in promoting sterile inflammation. ATP is the ligand for P2X7 and is stored at high concentrations (5–10 mM) in most cells (6). During MI/R, disruption of coronary blood flow causes cell damage, leading to a massive release of ATP. Following ATP into the extracellular space, CD39 converts ATP into AMP and regulates ATP concentrations. Once the line is crossed, ATP becomes a potent damage-associated molecular pattern, binds P2X7, and triggers cell death (7). Furthermore, P2X7 plays a role in regulating the homeostasis of metabolism and immunity in diabetes (1). Most studies have explored alterations of P2X7 in diabetic nephropathy (8), retinopathy (9), and neuropathy (10), but the effect of diabetes on P2X7 expression and function of ischemic disease in the heart is unclear. Thus, it is important to understand whether P2X7 is involved in the pathogenesis of diabetes-aggravated MI/R injury. Identification of the specific functions of P2X7 in diabetes and the downstream molecules it activates will support evidence-based treatment design in diabetes-specific conditions.

In the present study, we assessed the vulnerability of MI/R injury in diabetic mice and then focused on the differences in the expression of P2X7 and its downstream molecules. We found that the major trigger of increased P2X7 was the MI/R-induced recruitment of monocytes macrophages, and diabetes can be a synergistic factor in this process. Therefore, we hypothesized that inhibition of P2X7

*Department of Anesthesiology, Zhujiang Hospital, Southern Medical University, Guangzhou, China; and †Department of Anesthesiology, Huazhong University of Science and Technology Union Shenzhen Hospital, Shenzhen, China

[1]F.W. and H.W. contributed equally to this work.

ORCID: 0000-0002-2613-0036 (S.X.).

Received for publication November 11, 2022. Accepted for publication March 20, 2023.

This work was supported by a grant from the National Natural Science Foundation of China (81771315)

S.X. conceived and designed the study. F.W. and H.W. conducted the research. Y.H. and J.G. analyzed the data. S.X. and F.W. wrote the manuscript. All authors read and approved the final manuscript.

Address correspondence and reprint requests to Shiyuan Xu, Department of Anesthesiology, Zhujiang Hospital, Southern Medical University, No. 253 Gongye Avenue, Guangzhou, P.R. China 510282. E-mail address: xsy998@smu.edu.cn

The online version of this article contains supplemental material.

Abbreviations used in this article: BBG, brilliant blue G; CK-MB, creatine kinase-MB; DM, diabetic mice; EF, left ventricular ejection fraction; FS, shortening fraction; HFD, high-fat diet; LSCI, laser speckle contrast imaging; LAD, left anterior descending coronary artery; MI/R, myocardial ischemia–reperfusion; NGF, nerve growth factor; NLRP3, nucleotide-binding oligomerization domain-like receptors family pyrin domain-containing 3; non-DM, nondiabetic mice; STZ, streptozotocin; TTC, triphenyltetrazolium chloride.

may overcome increased susceptibility of MI/R in diabetic mice. To validate this hypothesis, pharmacological enhancement and blockade of P2X7 using BzATP, brilliant blue G (BBG), and A438079, respectively, were used to investigate the role of P2X7 in aggravated MI/R injury. Of note, both 2 wk of BBG injection before MI/R and acutely administered A438079 at the time of MI/R injury alleviated cardiac injury in diabetic mice.

Materials and Methods

Ethics statement

All animal experiments were approved by the Animal Ethics Committee of Zhujiang Hospital, Southern Medical University (Project Number LAEC-2021-101).

Induction of diabetes

The specific pathogen-free and 4-wk-old male C57BL6/J mice were bought from Guangdong Sijiajingda Biotechnology Co. Mice were placed in a dedicated pathogen-free facility with controlled temperature and humidity with a 12-h/12-h light/dark cycle and ad libitum access to water and standard laboratory rodent chow or 60% high-fat fodder. The fodder was purchased from Guangdong Medical Laboratory Animal Center. The high-fat diet (HFD) and streptozotocin (STZ)-induced diabetic mouse model was developed as previously described (11). Briefly, 4-wk-old male C57BL6/J mice were fed an HFD (60% fat) for 8 wk to induce diabetes. Age-matched nondiabetic mice were fed a standard normal diet for 8 wk. STZ (Sigma-Aldrich, St. Louis, MO) was dissolved in sodium citrate buffer and injected (100 mg/kg, one dose, i.p. injection) into 8-wk-old mice, and 12-wk-old mice were fasted for 6 h (from 8:00 to 14:00). Blood glucose was quantified from a tail-vein blood sample using a Freestyle blood glucose monitoring system (Abbott). The 12-wk-old mice with blood glucose levels above 11.1 mmol/L were considered diabetic mice.

MI/R

After i.p. injection of sodium pentobarbital (50 mg/kg), the trachea was intubated and connected to a small animal ventilator (RoVent Jr. Small Animal Ventilator, Kent Scientific). MI/R was performed by tying the left anterior descending coronary artery (LAD) using an 8-0 silk suture slipknot. Thirty minutes after ischemia, the slipknot was released, and reperfusion of the myocardium was performed for 24 h.

Definition and harvest of cardiac injury region

Cardiac tissue regions were defined as the ischemic zone (left ventricular free wall), border zone (left ventricular anterior and posterior wall), and distal zone (interventricular septum) (12). The cardiac apex corresponds to the left ventricle, which was also the main infarct area. In our study, the cardiac apex below the ligation site was harvested 24 h after reperfusion and was used for the Western blots, immunofluorescence, immunohistochemistry, and flow cytometry.

Administration of drugs

BBG (S3217, Selleck), a P2X7 receptor antagonist, was diluted at 3 mg/ml in vehicle (saline) solution and injected i.p. Briefly, mice were administered BBG (45.5 mg/kg) every 48 h (once per day) for 2 wk, and the final BBG treatment was performed 30 min before MI/R (13). A438079 (HY-15488A, MedChemExpress), a selective P2X7 antagonist, was administered by i.p. injection (diluted at 100 mg/ml in vehicle [saline] solution, 100 mg/kg) 30 min after MI/R (14, 15). In addition, 0.1 μg/μl BzATP triethylammonium salt (ab120444, Abcam, Cambridge, UK), a P2X7 agonist, was administered 3 μl/mouse before the slipknot was released (16).

Laser speckle contrast imaging (LSCI) of ischemic hearts

Left ventricular blood flow was quantitatively measured by LSCI (SIM BFI-HR Pro, Wuhan XunWei Optoelectronic Technology), as previously described by Kavanagh et al. (17). In brief, mice were surgically molded, and an LSCI device was placed above the exposed heart. A defined area was delineated with the left ventricle to observe blood flow downstream of the LAD ligation site to help determine the success of the ligation.

Myocardial tissue staining

Myocardial infarct size was determined by Evans blue (Sigma-Aldrich)/triphenyltetrazolium chloride (TTC) (Sigma-Aldrich) staining. In brief, the LAD was religatured in the previous location following 24 h of reperfusion, and 1.5% Evans blue was injected into the ascending aorta. The heart was sliced, incubated in 1% TTC at 37°C for 15 min, and photographed. The Evans blue–negative staining area of the myocardium indicated the area at risk, and the TTC-negative staining portion indicated the infarct. Myocardial infarct size was expressed as a percentage of the infarct area over risk area.

Echocardiography and electrocardiogram analysis

After inhalation of 1.5% isoflurane, mice were monitored by echocardiography and electrocardiogram. Ventricular function was measured by the VisualSonics Vevo 3100 imaging system (Fujifilm Corporation). Short-axis two-dimensional echocardiography of the ventricle was collected on the maximum transverse surface of the left ventricle, including two papillary muscles in a constant position. Left ventricular ejection fraction (EF) and shortening fraction (FS) were calculated by Vevo LAB software. The BIOPAC MP160 system (BIOPAC Systems) was used to continuously monitor electrocardiograms every 5 min in mice, and the data were analyzed by AcqKnowledge software.

Measurements of creatine kinase-MB (CK-MB) and total cholesterol

Serum CK-MB level was determined using a commercially available mouse ELISA kit (Nanjing Jiancheng Bioengineering Institute). Total cholesterol was measured by a mouse total cholesterol ELISA kit (Shanghai Enzyme-linked Biotechnology). Both experiments were based on the manufacturer's instructions.

Histochemical analysis and apoptosis determination

Each sample was embedded in paraffin, cut into 5-μm-thick sections, and stained with the following primary Abs: P2X7 (ab259942, 1:1000, Abcam) and Iba-1 (ab178847, 1:1000, Abcam). Apoptosis was measured by TUNEL assay, using a commercial kit according to the manufacturer's protocol (KeyGEN Biotech). ImageJ software was used to count positive cells, which were expressed as a percentage of positive cells. The percentage of TUNEL-positive nuclei among total nuclei was calculated to determine the apoptosis index.

Immunofluorescence

Myocardial localization of P2X7 and F4-80 were identified by immunofluorescence using the following Abs: P2X7 (ab259942, 1:250, Abcam), F4-80 (ab6640, 1:1000, Abcam), goat anti-rabbit IgG H&L (Alexa Fluor 594, Abcam), and goat anti-rat IgG H&L (Alexa Fluor 488, Abcam). The fluorescence was observed under a fluorescence microscope (TS100, Nikon).

Western blot analysis

Proteins were separated on a 10% or 12% $NaDodSO_4$–PAGE SDS-PAGE gel and transferred to a polyvinylidene fluoride (ISEQ00010, IPVH00010, MerckMillipore) membrane. Membranes were blocked with 5% nonfat milk for 1 h and then incubated with the following primary Abs overnight at 4°C: P2X7 (ab259942, 1:2000, Abcam), NLRP3 (NBP1-77080, 1:1000, Novus Biologicals), caspase-1 (24232, 1:500, Cell Signaling Technology), IL-1β (ab254360, 1:500, Abcam), CD39 (14481, 1:1000, Cell Signaling Technology), caspase-3 (14220, 1:500, Cell Signaling Technology), IL-10 (AF519, 1:500, R&D Systems, Minneapolis, MN), tyrosine hydroxylase (25859-1-AP, 1:2000, Proteintech, Rosemont, IL), and β-tubulin (AP0064, 1:5500, Bioworld). The results were analyzed by ImageJ software.

Quantitative real-time PCR analysis

NGF mRNA expression was assessed by quantitative real-time PCR with the following primer sequences: 5′-AGACTCCACTCACCCCGTG-3′ (forward primer) and 5′-GGCTGTGGTCTTATCTCCAAC-3′ (reverse primer). Total RNA was extracted from myocardial tissue using TRIzol reagent (Accurate Biology), and reverse transcription and amplification were performed using a SYBR Green kit (RR820A, Takara). All data were normalized to β-actin under the same conditions by the comparative cycle threshold method.

Flow cytometry

In order to prepare single-cell suspensions from infarct tissue, 50 mg tissue of the cardiac apex was harvested under aseptic conditions, washed in HBSS, ground up with scissors, placed into a mixture of collagenase type I (Thermo Fisher, Waltham, MA) and dispase II (Sigma-Aldrich), and digested at 37°C for 45 min. The cells were then centrifuged (15 min, 1200 × *g*, 4°C) and filtered through 40-μm nylon filters (BD Biosciences, San Jose, CA).

For extracellular staining, 1×10^6 cells were resuspended in 100 μl PBS/2% BSA and costained for cell surface P2X7, CD45, CD11b, Ly6G, and Ly6C. The cell suspensions were incubated with the following primary Abs for 30 min at room temperature: PE anti-mouse P2X7R (148703, 0.25 μg/100 μl), FITC anti-mouse CD45 (103107, 1:100), PerCP/cyanine 5.5 anti-mouse/human CD11b (101227, 0.25 μg/100 μl), allophycocyanin anti-mouse Ly6G (127613, 0.06 μg/100 μl), Brilliant Violet 421TM anti-mouse Ly6C (128031, 1:20), all Abs from BioLegend. Data were acquired on a FACSCalibur cytometer (CytoFLEX, Beckman Coulter, Indianapolis, IN). The results were analyzed

by FlowJo version 10.8.1 software and were expressed as a percentage of cells within the selected gate among total cells.

Statistical analysis

All data are expressed as mean ± SEM. $p < 0.05$ was considered statistically significant. The Student t test or two-way ANOVA with post hoc testing (Bonferroni) was used to compare differences between groups. Statistical analysis was performed using Prism version 9.0 software (GraphPad Software, La Jolla, CA).

Results

Mouse model of MI/R and diabetes

Echocardiography and LSCI were used to determine the stability of the MI/R model. The Echocardiography showed a significant elevation of the ST segment after ligation of the LAD. LSCI showed a deep blue color at the cardiac apex, indicating substantial decreased ventricular blood flow (Supplemental Fig. 1). The blood glucose was significantly increased in the diabetic mice compared with the nondiabetic mice at 12 wk (Fig. 1A; 13.51 ± 0.40 mmol/L versus 5.61 ± 0.08 mmol/L; $p < 0.0001$). The body weight was higher in diabetic mice at 12 wk (Fig. 1B; 32.49 ± 0.64 g versus 26.22 ± 0.46 g; $p < 0.0001$). Serum total cholesterol of diabetic mice was obviously elevated (Fig. 1C; 3.44 ± 0.11 mmol/L versus 1.42 ± 0.12 mmol/L; $p < 0.0001$).

P2X7 and CD39 expression in HFD/STZ-induced diabetes mice

Myocardial P2X7 levels increased at the 12th week in diabetic mice (Fig. 1E; diabetic mice [DM] [12 wk] versus non-DM [12 wk]; $p < 0.05$). There was no significant difference in P2X7 expression at the 10th, 12th, and 14th weeks in diabetic mice (Fig. 1E; DM [10 wk] versus DM [12 wk]; ns; DM [12 wk] versus DM [14 wk]; ns; DM [10 wk] versus DM [14 wk]; ns). Myocardial CD39 expression showed a significant increase at the 12th week in diabetic mice compared with nondiabetic mice (Fig. 1F; DM [12 wk] versus non-DM [12 wk]; $p < 0.05$). There was a significant increase of CD39 at the 14th week in diabetic mice compared with other time points (Fig. 1F; DM [14 wk] versus DM [12 wk]; $p < 0.001$; DM [14 wk] versus DM [10 wk]; $p < 0.01$).

Characterization of MI/R injury in diabetic mice

Compared with the non-DM I/R group, the DM I/R group showed a larger infarct area (Fig. 2C; 0.35 ± 0.01 versus 0.54 ± 0.05; $p < 0.01$), without a statistically significant difference in the myocardial infarction risk area (Fig. 2B; 0.53 ± 0.04 versus 0.51 ± 0.05; ns). Moreover, there was no significant difference in ventricular contractile function between the sham groups (Fig. 2E, 2F; non-DM sham group versus DM sham group: EF, 68.62 ± 2.66% versus 69.24 ± 3.25%; ns; FS, 37.87 ± 2.00% versus 38.39 ± 2.60%; ns), and the decreases in EF (non-DM I/R group versus DM I/R group: 52.26 ± 2.12% versus 44.66 ± 0.92%; $p < 0.05$) and FS (non-DM I/R group versus DM I/R group: 26.41 ± 1.46% versus 21.69 ± 0.53%; $p < 0.05$) were more evident in the diabetic mice after MI/R. Serum CK-MB levels were further elevated in the DM I/R group compared with the non-DM I/R group (Fig. 2I; 197.3 ± 20.37 U/L versus 285.6 ± 21.92 U/L; $p < 0.01$). Additionally, the DM I/R group had increased apoptosis (Fig. 2H; 11.35 ± 0.72% versus 24.83 ± 3.75%; $p < 0.05$).

Infiltration levels and cell types of immune cells after MI/R in diabetic mice

After 24 h of reperfusion, immunohistochemistry showed extensive macrophage infiltration after MI/R in the diabetic mice (Fig. 3A; DM I/R group versus non-DM I/R group; $p < 0.05$). Flow cytometry was used to investigate the infiltration levels and cell types of immune cells after MI/R in diabetic mice. The percentages of leukocytes ($CD45^+$ cells), myeloid cells ($CD45^+$ $CD11b^+$ cells), monocytes and macrophages ($CD45^+$ $CD11b^+$ $Ly6G^-$ Ly6C cells), and neutrophils ($CD45^+$ $CD11b^+$ $Ly6G^+$ cells) were significantly higher in I/R groups than in the sham group (Fig. 3C–3G; DM I/R group versus DM sham group; $p < 0.0001$, $p < 0.0001$, $p < 0.0001$, and $p < 0.0001$, respectively; non-DM I/R group versus non-DM sham group, $p < 0.0001$, $p < 0.0001$, $p < 0.0001$, and

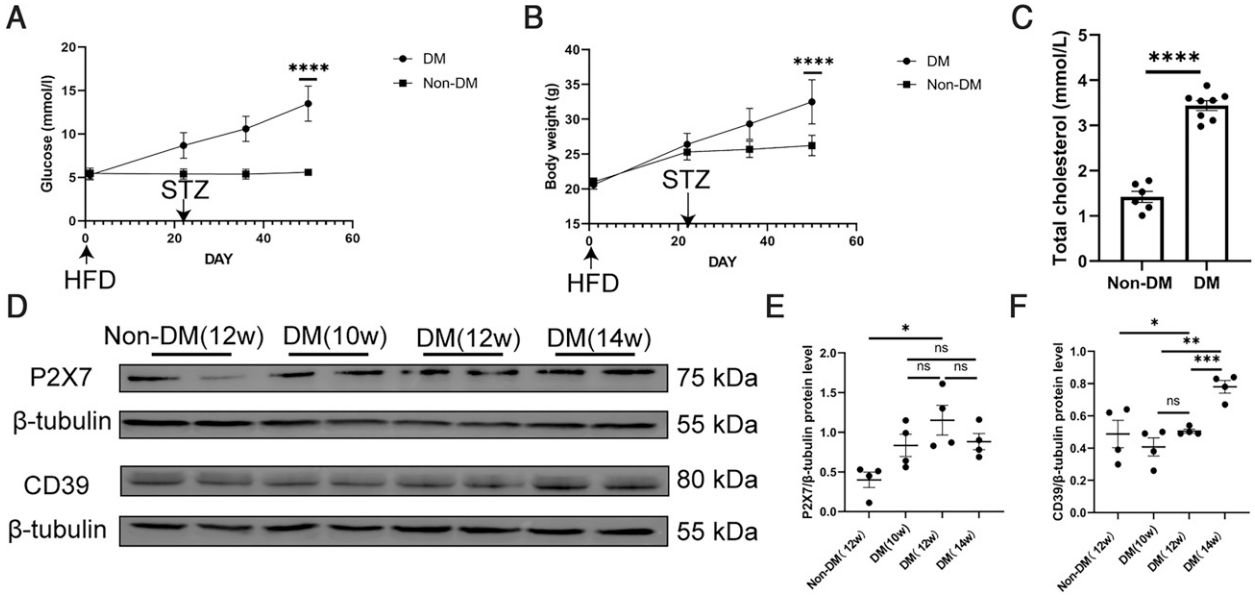

FIGURE 1. Blood glucose, body weight, total cholesterol, P2X7, and CD39 levels in diabetic and nondiabetic mice. (**A**) Blood glucose of diabetic mice ($n = 100$) and nonpatients with diabetes mice ($n = 50$) at 4 wk, 8 wk, and 12 wk after HFD/normal diet. (**B**) Body weight of diabetic mice ($n = 100$) and nonpatients with diabetes mice ($n = 50$) at 4 wk, 8 wk, and 12 wk after HFD/normal diet. (**C**) Serum total cholesterol of diabetic mice ($n = 8$) and nondiabetic mice ($n = 6$). (**D**) Western blot of myocardial P2X7 and CD39 in 12-wk-old nondiabetic mice ($n = 4$) and in 10-wk-, 12-wk-, and 14-wk-old diabetic mice ($n = 4$). (**E**) Quantitative analysis of P2X7. (**F**) Quantitative analysis of CD39. *$p < 0.05$, **$p < 0.01$, ***$p < 0.001$, ****$p < 0.0001$.

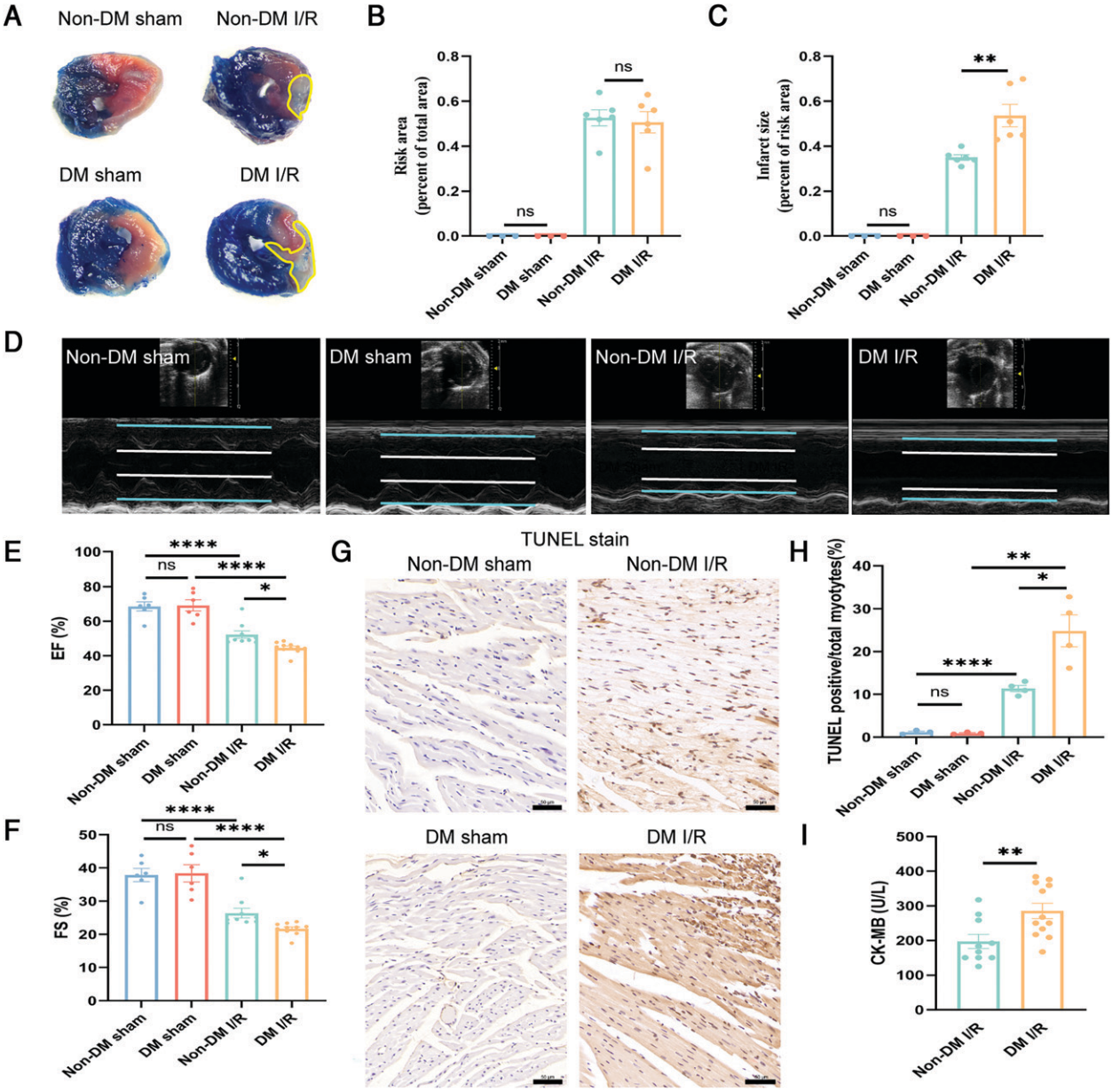

FIGURE 2. Characteristics of MI/R injury in diabetic mice. (**A**) The infarct size was determined by Evans blue/TTC staining. (**B**) Postischemia risk area expressed as a percentage of risk area to the total area (n = 3–6). (**C**) Postischemia infarct size expressed as a percentage of infarct size to the area at risk (n = 3–6). (**D**) Representative M-mode echocardiographic images. (**E**) EF (n = 6–11). (**F**) FS (n = 6–11). (**G**) TUNEL staining. Scale bar, 50 μm. (**H**) TUNEL positive/total myocytes (n = 3 or 4). (**I**) Plasma CK-MB levels (n = 10–12). *$p < 0.05$, **$p < 0.01$, ****$p < 0.0001$. DM I/R, diabetic mice with MI/R operation; DM sham, diabetic mice with sham operation; Non-DM I/R, nondiabetic mice with MI/R operation; Non-DM sham, nondiabetic mice with sham operation.

$p < 0.01$, respectively). Diabetes further deteriorated the infiltration of these cells (Fig. 3C–3G; DM I/R group versus non-DM I/R group, $p < 0.0001$, $p < 0.0001$, $p < 0.001$, and $p < 0.01$, respectively).

P2X7 signals and inflammation in diabetic mice after MI/R

In response to MI/R, myocardial P2X7 expression was further upregulated in diabetic mice (Fig. 4B; DM I/R group versus non-DM I/R group, $p < 0.01$), and myocardial P2X7 expression was elevated in the MI/R group compared with the sham group (Fig. 4B; DM I/R group versus DM sham group, $p < 0.05$; non-DM I/R group versus non-DM sham group, $p < 0.05$). Immunohistochemistry showed that P2X7 was overexpressed in diabetic conditions (Fig. 4D; DM I/R group versus non-DM I/R group, $p < 0.01$; DM sham group versus non-DM sham group, $p < 0.01$). To determine ATP hydrolysis, we found that CD39 expression was higher in the DM I/R group than in the non-DM I/R group (Fig. 4C; $p < 0.0001$) and that CD39 expression was upregulated in the MI/R group compared with the sham group (Fig. 4C; DM I/R group versus DM sham group, $p < 0.001$; non-DM I/R group versus non-DM sham group, $p < 0.01$). We next investigated the correlation between the NLRP3/caspase-1/IL-1β axis and P2X7 activation. The protein levels of NLRP3, pro-caspase-1, cleaved caspase-1, pro-IL-1β, and IL-1β were significantly increased in the DM I/R group compared with the non-DM I/R group (Fig. 4F, 4G; $p < 0.01$, $p < 0.01$, $p < 0.01$, $p < 0.05$, and $p < 0.01$, respectively), and these levels were low in the sham group (Fig. 4F, 4G; DM I/R group versus DM sham group, $p < 0.01$, $p < 0.0001$, $p < 0.05$, $p < 0.01$, and $p < 0.05$, respectively; non-DM I/R group versus non-DM sham group, $p < 0.05$, $p < 0.0001$, $p < 0.05$, $p < 0.05$, and $p < 0.05$, respectively).

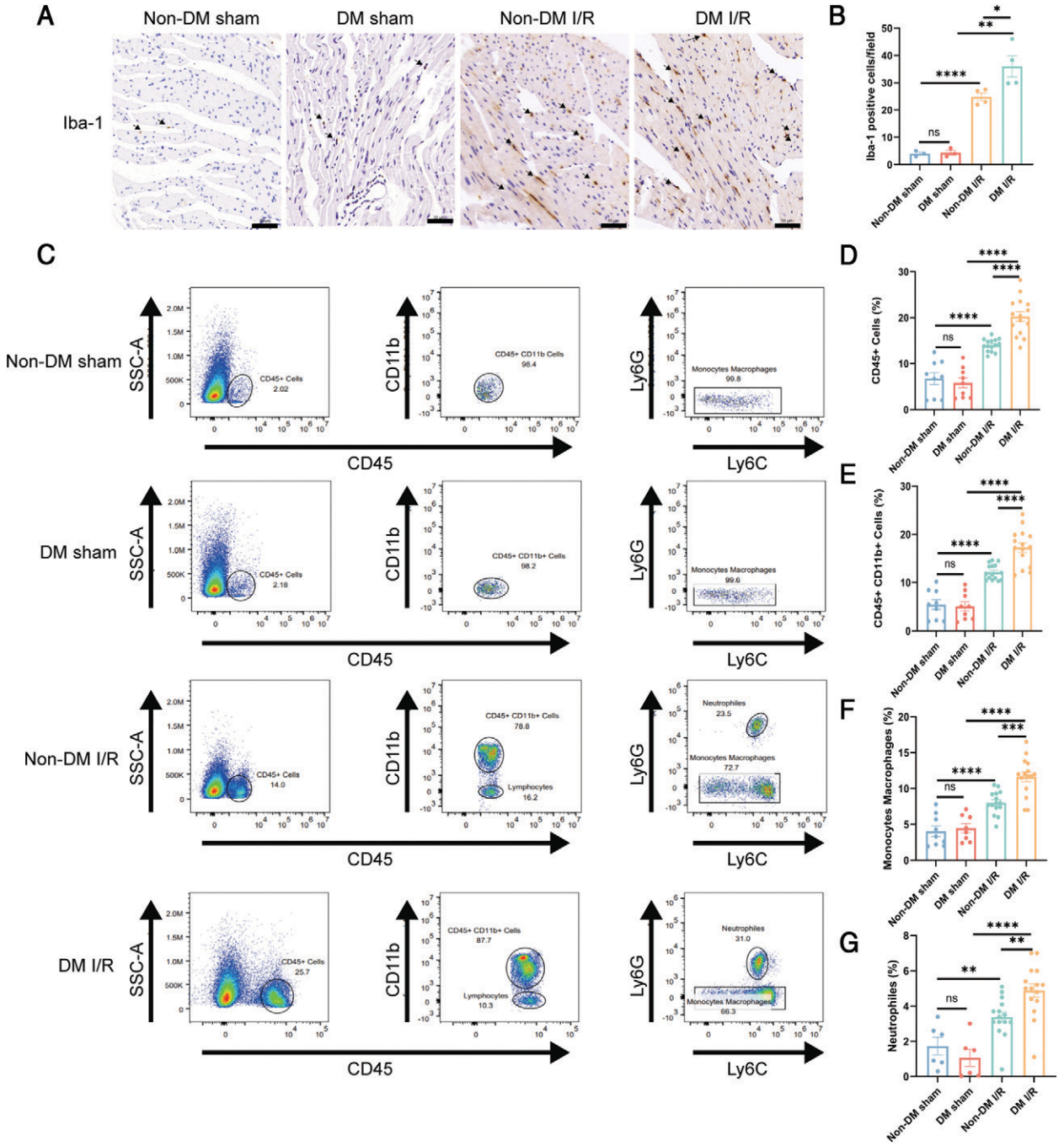

FIGURE 3. Infiltration levels and cell types of immune cells. (**A**) Immunohistochemical detection of Iba-1. Scale bar, 50 μm. (**B**) Iba-1-positive nuclei/total nuclei (n = 3 or 4). (**C**) Flow cytometric gating strategy and quantification of monocytes and macrophages of infarcted areas 24 h after MI/R. (**D–G**) Flow cytometric quantification of $CD45^+$ cells, $CD45^+$ $CD11b^+$ cells, monocytes, macrophages, and neutrophils (n = 6–15). *$p < 0.05$, **$p < 0.01$, ***$p < 0.001$, ****$p < 0.0001$. DM I/R, diabetic mice with MI/R operation; DM sham, diabetic mice with sham operation; Non-DM I/R, nondiabetic mice with MI/R operation; Non-DM sham, nondiabetic mice with sham operation; SSC-A, side scatter area.

Upregulated P2X7 was mainly expressed in monocytes and macrophages

As shown in Fig. 4H–4K, we found that the percentage of $P2X7^+$ cells was elevated after 24 h of reperfusion, especially in the DM I/R group (non-DM I/R group versus non-DM sham group, $p < 0.0001$; DM I/R group versus DM sham group, $p < 0.0001$; DM I/R group versus non-DM I/R group, $p < 0.001$). The percentage of $P2X7^+$ $CD45^+$ $CD11b^+$ cells was high in $P2X7^+$ cells (non-DM sham group, 80.06 ± 2.53%; DM sham group, 82.08 ± 2.46%; non-DM I/R group, 80.08 ± 2.31%; DM I/R group, 84.41 ± 1.17%). Furthermore, the main cell type of $P2X7^+$ $CD45^+$ $CD11b^+$ cells was $P2X7^+$ $CD45^+$ $CD11b^+$ $Ly6G^-$ Ly6C cells (non-DM sham group, 98.15 ± 0.34%; DM sham group, 84.81 ± 2.67%; non-DM I/R group, 96.70 ± 1.95%; DM I/R group, 97.96 ± 0.53%). Immunofluorescence staining also suggested that P2X7 could be located near F4-80 (see Supplemental Fig. 3).

The role of P2X7 in diabetes-aggravated MI/R injury

The results described above indicated that the DM I/R group had more severe MI/R injury and higher expression of P2X7 than the non-DM I/R group. We further used BzATP in nondiabetic mice to investigate if it could eliminate this effect. BzATP increased myocardial P2X7 expression in nondiabetic mice and led to no significant

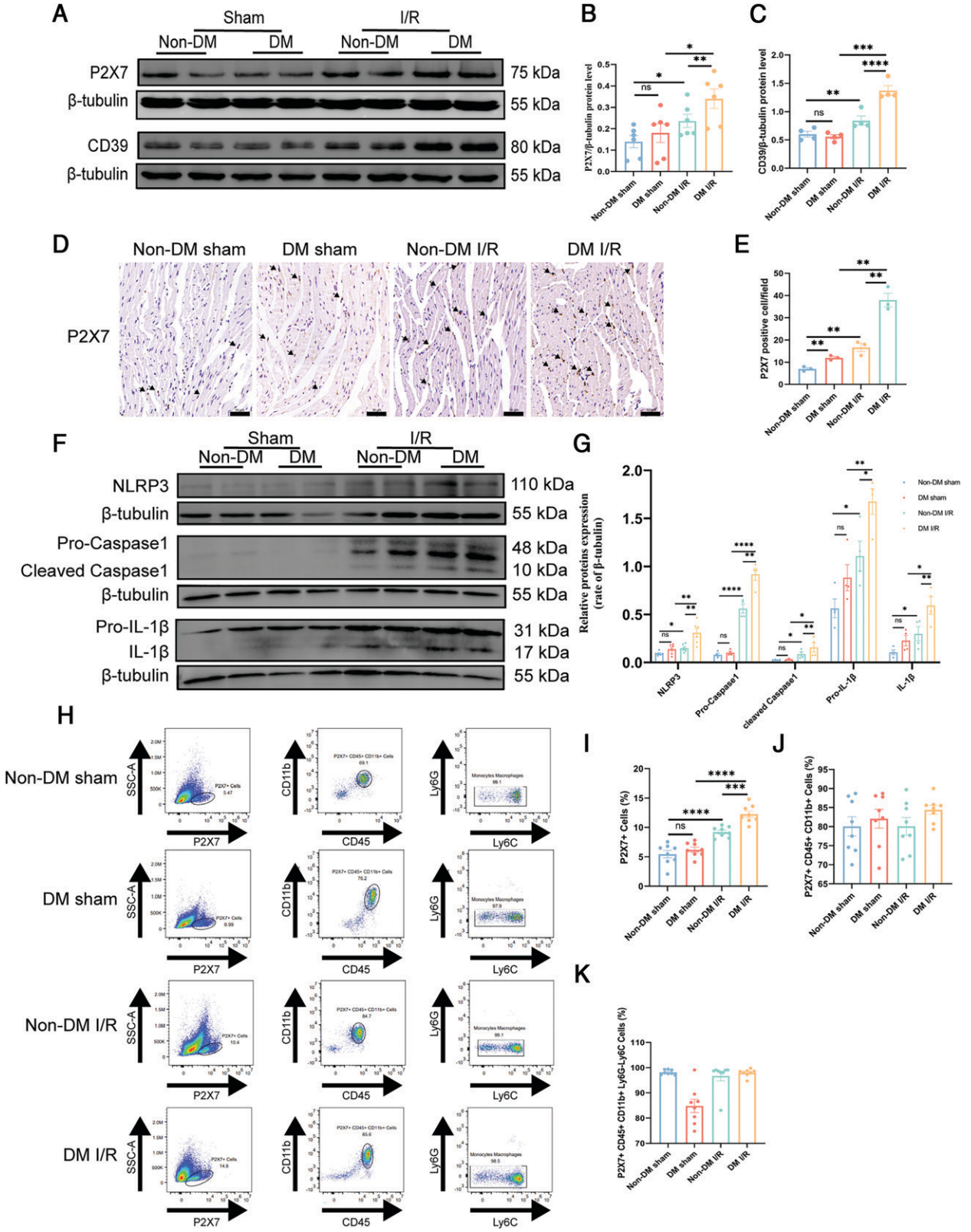

FIGURE 4. P2X7 expression and location after MI/R. (**A**) Representative Western blot of P2X7 and CD39. (**B**) Quantitative data of P2X7 ($n = 6$). (**C**) Quantitative data of CD39 ($n = 4$). (**D**) Immunohistochemical detection of P2X7. Scale bar, 50 μm. (**E**) P2X7 positive/total myocytes ($n = 3$). (**F**) Representative Western blot of NLRP3, pro-caspase-1, cleaved caspase-1, pro-IL-1β, and IL-1β. (**G**) Quantitative analysis of NLRP3, pro-caspase-1, cleaved caspase-1, pro-IL-1β, and IL-1β ($n = 4$–6). (**H**) Flow cytometric gating strategy and quantification of $P2X7^+$ cells of infarcted areas 24 h after MI/R. (**I**–**K**) Flow cytometric quantification of $P2X7^+$ cells, $P2X7^+$ $CD45^+$ $CD11b^+$ cells, $P2X7^+$ $CD45^+$ $CD11b^+$ $Ly6G^-$ Ly6C cells ($n = 8$). $^*p < 0.05$, $^{**}p < 0.01$, $^{***}p < 0.001$, $^{****}p < 0.0001$. DM I/R, diabetic mice with MI/R operation; DM sham, diabetic mice with sham operation; Non-DM I/R, nondiabetic mice with MI/R operation; Non-DM sham, nondiabetic mice with sham operation.

difference with diabetic mice (Fig. 5A, 5B; non-DM I/R+BzATP group versus DM I/R group; ns). Furthermore, there was no significant difference in myocardial infarction area (Fig. 5E, 5F; non-DM I/R+BzATP group versus DM I/R group: risk area, 0.35 ± 0.03 versus 0.43 ± 0.03, ns; infarct size, 0.47 ± 0.06 versus 0.56 ± 0.04, ns), EF (Fig. 5H, 5I; non-DM I/R+BzATP group versus DM I/R group: EF, 47.56 ± 2.28% versus 43.25 ± 3.71%, ns; FS, 23.47 ± 1.35% versus 20.75 ± 2.06%, ns), serum CK-MB (Fig. 5C; non-DM I/R+BzATP group versus DM I/R group: 313.2 ± 15.01 U/L versus 332.3 ± 59.84 U/L, ns), and the 3-d survival rate (Fig. 5J; non-DM I/R+BzATP group versus DM I/R group: 44.44% versus 46.67%, $p = 0.08$). On the basis of these results, we believed that BzATP eliminated the differences between diabetic and nondiabetic mice in MI/R injury. Notably, BBG downregulated myocardial P2X7 expression (Fig. 5B; DM I/R group versus DM I/R+BBG group, $p < 0.05$). BBG treatment in diabetic mice not only inhibited infarct area (Fig. 5E, 5F; DM I/R group versus DM I/R+BBG group: risk area, 0.43 ± 0.03 versus 0.45 ± 0.03, ns; infarct size, 0.56 ± 0.04 versus 0.31 ± 0.04, $p < 0.001$), decreased serum CK-MB levels (Fig. 5C; DM I/R group versus DM I/R+BBG group: 332.3 ± 59.84 U/L versus 192.3 ± 23.56 U/L, $p < 0.05$), and improved ventricular systolic function (Fig. 5H, 5I; DM I/R group versus DM I/R+BBG group: EF, 43.25 ± 3.71% versus 57.64 ± 2.68%, $p < 0.05$; FS, 20.75 ± 2.06% versus 29.66 ± 1.71%, $p < 0.05$) but also improved the 3-d survival rate (Fig. 5J; DM I/R group versus DM I/R+BBG group: 46.67% versus 82.35%, $p = 0.04$). BBG treatment did not affect the weight or blood glucose in diabetic mice (see Supplemental Fig. 2). In addition, 2-wk administration of BBG in nondiabetic mice also alleviated cardiac injury and inhibited the recruitment of immune cells (see Supplemental Fig. 4).

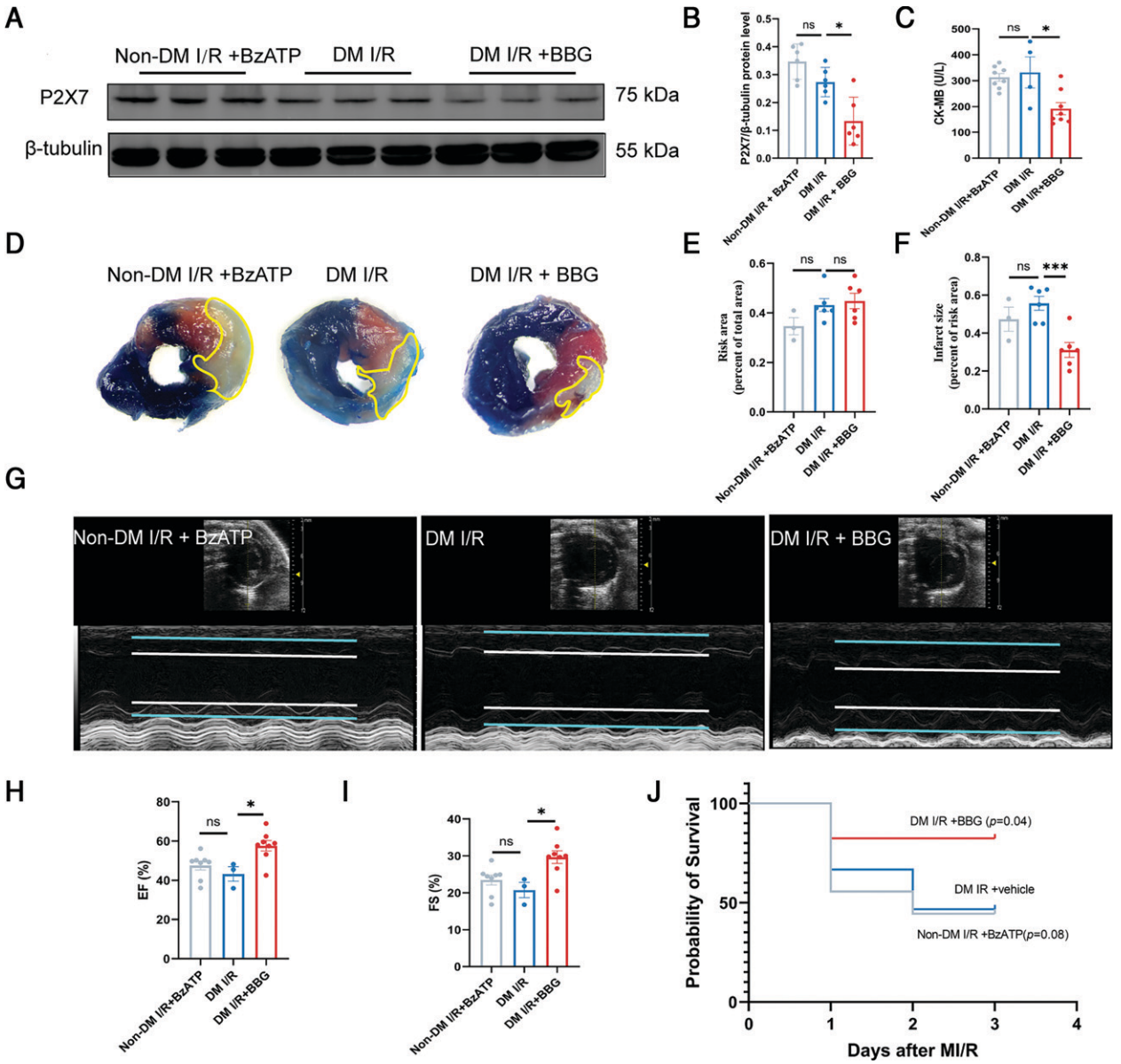

FIGURE 5. Inhibitor and agonist of P2X7 attenuated or aggravated MI/R injury. (**A**) Representative Western blot shows the effect of BzATP and BBG on P2X7. (**B**) Quantitative analysis of P2X7 ($n = 6$). (**C**) Plasma CK-MB levels ($n = 4$–8). (**D**) Infarct size was determined by Evans blue/TTC staining. (**E**) Postischemia risk area expressed as a percentage of risk area to the total area ($n = 3$–6). (**F**) Postischemia infarct size expressed as a percentage of infarct size to the area at risk ($n = 3$–6). (**G**) Representative M-mode echocardiographic images. (**H**) EF ($n = 3$–8). (**I**) FS ($n = 3$–8). (**J**) Three-day survival rate ($n = 9$–17). *$p < 0.05$, ***$p < 0.001$. DM I/R, diabetic mice with MI/R operation; DM I/R + BBG, diabetic mice with BBG treatment and MI/R operation; Non-DM I/R+BzATP, nondiabetic mice with BzATP treatment and MI/R operation.

Effects of BzATP and BBG on NLRP3 and apoptosis

As shown in Fig. 6A–6F, BzATP eliminated the differences in NLRP3, pro-caspase-1, cleaved caspase-1, pro-IL-1β, and IL-1β expression between nondiabetic mice and diabetic mice after MI/R. BBG blockade of P2X7 effectively inhibited the NLRP3/caspase-1/IL-1β axis in diabetic mice ($p < 0.05$, $p < 0.01$, and $p < 0.05$, respectively). IL-10 was increased in the DM I/R + BBG group compared with the DM I/R group (Fig. 6G; $p < 0.05$). In addition, the non-DM I/R + BzATP group had no significant difference with the DM I/R group in myocardial apoptosis (Fig. 6H, 6I; 22.75 ± 2.10% versus 21.28 ± 2.21%, ns) and cleaved caspase-3 (Fig. 6J, 6L; ns). BBG decreased the incidence of myocardial apoptosis (Fig. 6H, 6I; 21.28 ± 2.21% versus 11.90 ± 0.51%, $p < 0.01$) and downregulated the expression of cleaved caspase-3 (Fig. 6L; $p < 0.05$).

Effects of administering A438079 30 min after reperfusion on diabetic mice

A438079 effectively reduced infarct area (Fig. 7A–7C; DM I/R group versus DM I/R + A438079 group: risk area, 0.51 ± 0.05 versus 0.54 ± 0.05, ns; infarct size, 0.53 ± 0.04 versus 0.35 ± 0.01, $p < 0.01$) and improved cardiac contractility (Fig. 7D–7F; DM I/R group versus DM I/R + A438079 group: EF, 45.17 ± 0.56% versus 52.59 ± 2.11%, $p < 0.01$; FS, 21.97 ± 0.35% versus 26.63 ± 1.44%, $p < 0.01$) in diabetic mice. In the results of Western blot analysis, there was low expression of P2X7, NLRP3, cleaved capase-1, IL-1β, and cleaved caspase-3 in the DM I/R + A438079 group (Fig. 7G–7L; DM I/R group versus DM I/R + A438079 group: $p < 0.0001$, $p < 0.001$, $p < 0.05$, $p < 0.05$, and $p < 0.01$).

BBG inhibited cardiac sympathetic nerve sprouts

As depicted in Fig. 8A, 8B, the heart rate significantly increased in the DM I/R group (DM I/R group versus baseline: 492.0 ± 24.17 beats/min versus 384.9 ± 9.95 beats/min, $p < 0.001$), but not in the DM I/R + BBG group (DM I/R + BBG group versus DM I/R group: 406.7 ± 8.66 beats/min versus 492.0 ± 24.17 beats/min, $p < 0.001$). We hypothesized that this may be associated with sympathetic nerve activity. To confirm this hypothesis, we found that the expression of tyrosine hydroxylase was higher in the DM sham group and DM IR group than in nondiabetic conditions (Fig. 8C, 8E; $p < 0.05$ and $p < 0.01$), which indicated that the sympathetic nerve was in an abnormally excited state in diabetes. These effects were reversed by BBG (Fig. 8D, 8F; $p < 0.05$). Immunohistochemical analysis showed significantly decreased macrophage recruitment in the DM I/R + BBG group (Fig. 8G, 8H; $p < 0.05$). Additionally, the NGF mRNA levels in the DM I/R + BBG group were lower (Fig. 8I; $p < 0.001$).

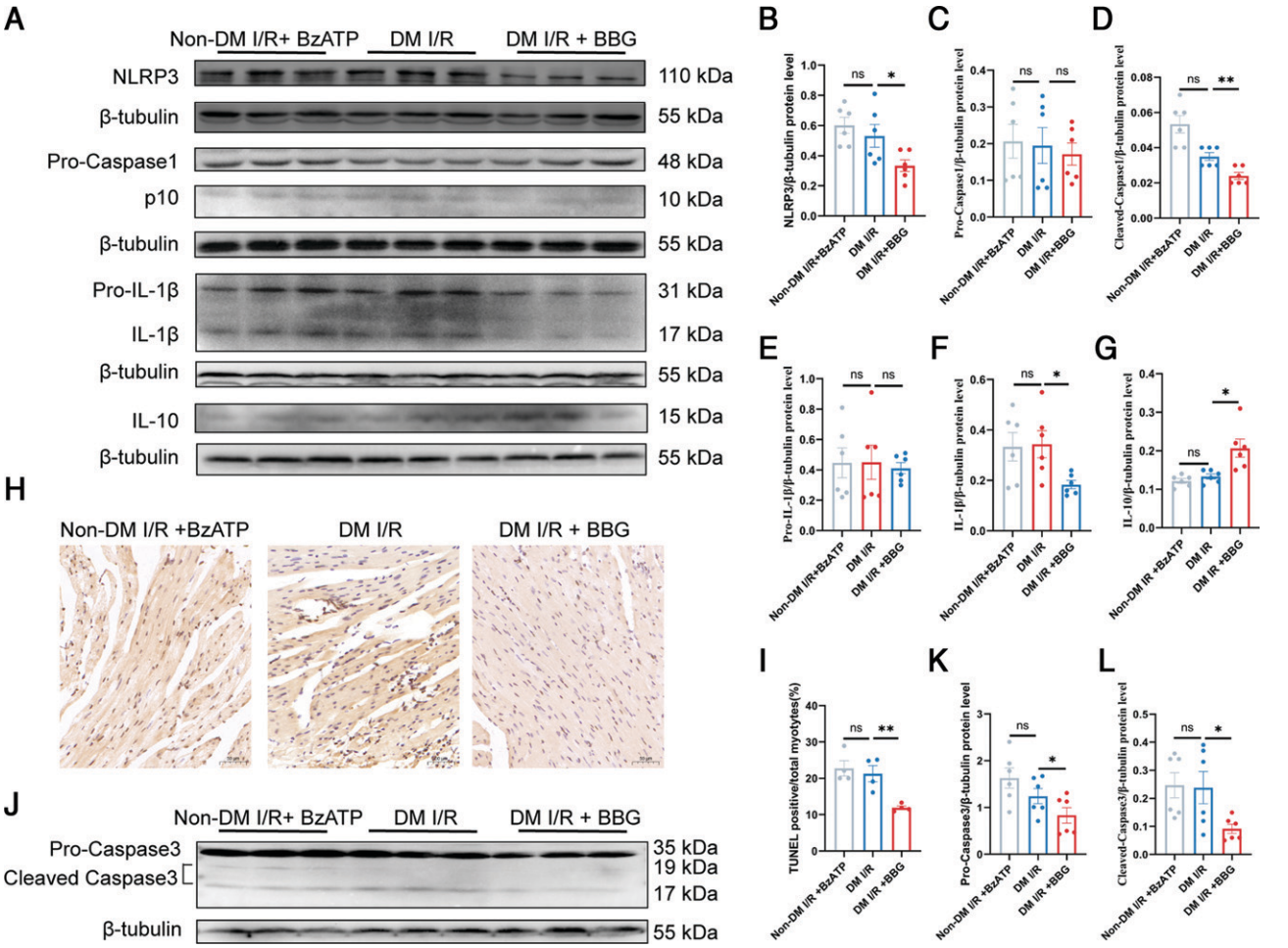

FIGURE 6. Effects of BBG and BzATP on NLRP3/caspase-1/IL-1β axis and apoptosis. (**A**) Representative Western blot of NLRP3, caspase-1, IL-1β, and IL-10. (**B–G**) Quantitative analysis of NLRP3, pro-caspase-1, cleaved caspase-1, pro-IL-1β, IL-1β, and IL-10 ($n = 6$). (**H**) TUNEL staining. Scale bar, 50 μm. (**I**) TUNEL-positive nuclei/total nuclei ($n = 4$). (**J**) Representative Western blot of caspase-3. (**K**) Quantitative analysis of pro-caspase-3 ($n = 6$). (**L**) Quantitative analysis of cleaved caspase-3 ($n = 6$). ns, $p > 0.05$; *$p < 0.05$; **$p < 0.01$. DM I/R, diabetic mice with MI/R operation; DM I/R + BBG, diabetic mice with BBG treatment and MI/R operation; Non-DM I/R+BzATP, nondiabetic mice with BzATP treatment and MI/R operation.

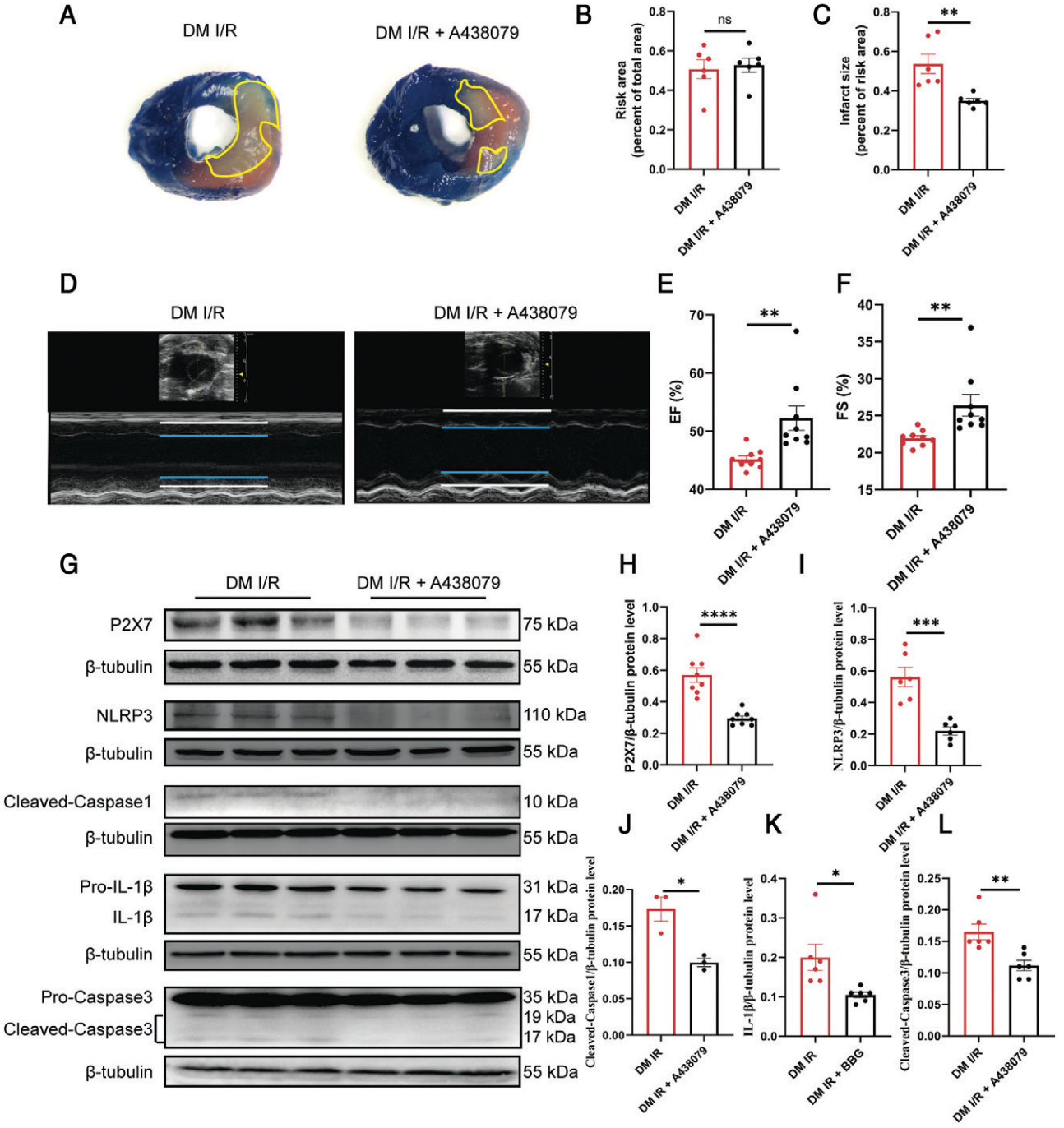

FIGURE 7. Effects of administering A438079 on diabetic mice after MI/R. (**A**) The infarct size was determined by Evans blue/TTC staining. (**B**) Postischemia risk area expressed as the percentage of risk area to the total area ($n = 6$). (**C**) Postischemia infarct size expressed as the percentage of infarct size to the area at risk ($n = 6$). (**D**) Representative M-mode echocardiographic images. (**E**) EF ($n = 9$). (**F**) FS ($n = 9$). (**G**) Representative Western blot of P2X7, NLRP3, cleaved caspase-1, pro-IL-1β, IL-1β, pro-caspase-3, and cleaved caspase-3. (**H–L**) Quantitative analysis of P2X7, NLRP3, cleaved caspase-1, IL-1β, and cleaved caspase-3 ($n = 3–8$). *$p < 0.05$, **$p < 0.01$, ***$p < 0.001$, ****$p < 0.0001$.

Discussion

Diabetes-aggravated MI/R injury remains an urgent medical issue, but a clear target is still lacking. Our study helps to explain the long-standing challenge of high cardiovascular morbidity and mortality in patients with diabetes. In the present study, we demonstrated that expression and function of P2X7 may be key to the relationship between the magnitude of cardiac damage and diabetes. Induction of diabetes was followed with the increased expression of P2X7. Moreover, P2X7 was further upregulated after MI/R in diabetic mice, thereby contributing to increased infarct size, ventricular function impairment, inflammation, and apoptosis. Finally, BBG blockade–decreased heart rate after MI/R may be related to inhibition of sympathetic nerve sprouts.

MI/R injury is partially driven by inflammation through multiple interacting pathways. Unfortunately, it is not limited to the heart, but altered by a variety of conditions, including comorbidities and age. To date, it is well accepted that a chronic, low-grade systemic inflammatory state is one innate component of diabetes (18, 19). Hyperglycemia-induced inflammation has been reported to contribute to the diastolic dysfunction in heart failure (20). Several preclinical and clinical studies strongly argue for anti-inflammatory treatment of diabetes (21). Hence, the inflammation can be a comechanistic

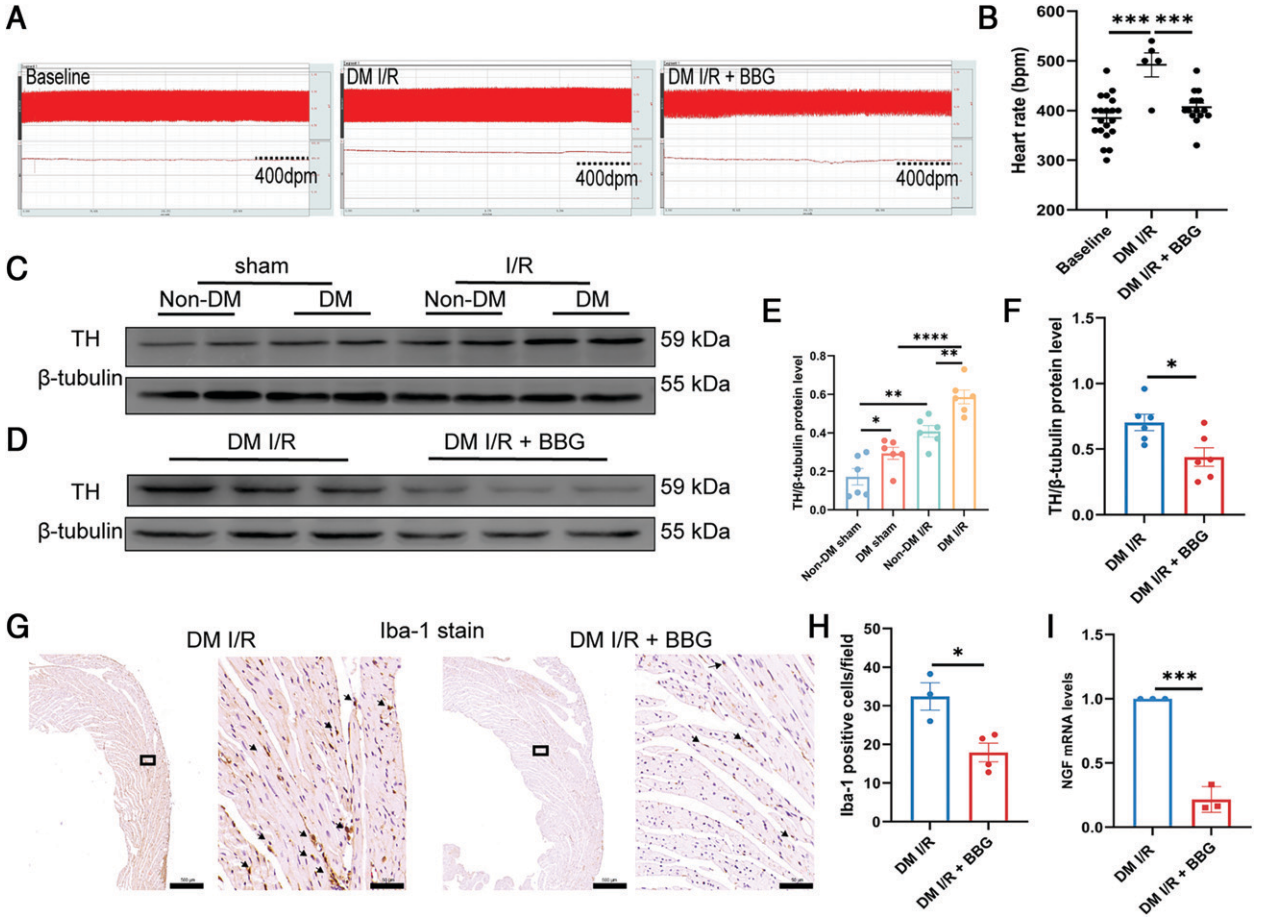

FIGURE 8. BBG-inhibited sympathetic nerve activity. (**A**) Representative tracings of heart rate. (**B**) Quantitative analysis of heart rate (n = 5–20). (**C**, **D**) Representative Western blot of tyrosine hydroxylase. (**E**, **F**) Quantitative analysis of tyrosine hydroxylase (n = 6). (**G**) Macrophage infiltration was evaluated by immunohistochemical detection of Iba-1. Scale bar, 500 μm or 50 μm. (**H**) Iba-1-positive nuclei/total nuclei (n = 3 or 4). (**I**) mRNA levels of NGF (n = 3). *$p < 0.05$, **$p < 0.01$, ***$p < 0.001$, ****$p < 0.0001$. DM I/R, diabetic mice with MI/R operation; DM I/R + BBG, diabetic mice with BBG treatment and MI/R operation; DM sham, diabetic mice with sham operation; Non-DM I/R, nondiabetic mice with MI/R operation; Non-DM sham, nondiabetic mice with sham operation.

approach related to diabetes and MI/R. Nonetheless, current effective and safe pharmacological treatments to reduce inflammation in diabetes MI/R are not sufficient. The Canakinumab Antibiotic Thrombosis Outcomes Study has shown that inhibition of IL-1β is effective in reducing the recurrence of cardiovascular events (22), but that it also suppresses the host response to infection (23). Comparatively, a P2X7 antagonist is superior due to its ability to block downstream effects beyond IL-1β and because it only binds to extracellular accumulating ATP, so it is unlikely to affect systemic immunosuppression due to additional off-target effects.

P2X7 has strong proinflammatory actions in response to ATP released from stress or apoptotic cells, and the results of flow cytometry showed that P2X7 was mainly expressed in $CD45^+$ $CD11b^+$ $Ly6G^-$ Ly6C cells (monocytes and macrophages) after 24 h of reperfusion. We found an increase in P2X7 expression after induction of diabetes, which is different from the situation in MI/R. In the normal heart, 45% were endothelial cells, 30% were cardiomyocytes, and less than 6% were immune cells (24). Hyperglycemia may impair coronary endothelial cells and expressed P2X7 (25). Hence, the upregulation of P2X7 after induction of diabetes may be related to endothelial cell damage caused by diabetic metabolic disorder. The same trend was observed in diabetic mice after MI/R, and P2X7 expression was correlated with increased NLRP3/caspase-1/IL-1β signals and macrophage recruitment. The increase of NLRP3 could further enhance the myocardial vulnerability, as previously reported (26). In fact, many kinds of cells in the heart can trigger NLRP3, whereas the intensity of stimulation and the effect of NLRP3 may be different. Studies have shown that the effects of NLRP3 activation in the heart are cell specific (27). For example, monocytes have many components of inflammatory substances and release large amounts of IL-1β at the lowest substrate; cardiomyocytes produce low levels of IL-1β; and NLRP3 shows low expression in most tissue-resident cells. Therefore, the cell types that induce more NLRP3 activation and large amounts of IL-1β release are more likely to be monocytes. In our study, we found that diabetic mice had more monocyte and macrophage infiltration, and P2X7 was mainly expressed in monocytes and macrophages after 30 min of reperfusion. Although we cannot rule out other factors that activate NLRP3, the increased P2X7-expressing monocytes and macrophages may significantly trigger the upregulation and activity of NLRP3 in our model. Taken together, the major trigger of increased P2X7 was the MI/R-induced recruitment of monocytes and macrophages, and diabetes can be a synergistic factor that promotes cells to release more ATP (28) and recruit more monocytes and macrophages, which activates NLRP3 assembly, promotes the maturation of IL-1β, and further accelerates inflammation amplification.

P2X7 contains a specific cytoplasmic domain without desensitization (29), and it causes persistent Ca^{2+} inflow and intracellular Ca^{2+} overload, which results in mitochondrial dysfunction, reactive oxygen species production, and suppression of ATP synthesis, ultimately inducing apoptosis. As our results showed, upregulation of P2X7 was significantly associated with cardiomyocyte apoptosis in diabetic mice,

and cleaved caspase-3 and cardiomyocyte apoptosis could be inhibited after BBG or A438079 treatment.

Cell lysis produces damage-associated molecular patterns, including ATP, which have been identified as a pathway that causes inflammation. However, this effect may be limited by CD39. Our study showed that either diabetes or MI/R increased CD39 expression. In fact, CD39 is just one indirect evidence reflecting extracellular ATP concentration (30), and increased P2X7 activity also directly promotes CD39 upregulation (30). In our study, we found that the upregulation of P2X7 was accompanied by increased CD39 at the 14th week in diabetic mice and a significant increase in CD39 in the DM I/R group, which indicated that a compensatory mechanism may exist: CD39 upregulation for degradation of excess extracellular ATP. Thus, CD39 is a key checkpoint that regulates the high extracellular ATP concentration and P2X7 activation in diabetes, but it does not offset P2X7 upregulation.

Intriguingly, our study showed that BBG blockade was linked with a slower heart rate after MI/R. It is known that the sympathetic nervous system regulates the heart rate, and abnormal cardiac sympathetic sprouts occur after myocardial infarction, which increases the incidence of arrhythmia (31). Macrophages are the central link between inflammation and sympathetic sprouting after myocardial infarction (32). Furthermore, diabetes is characterized by abnormal cardiac sympathetic activity (33). Hence, both MI/R and diabetes are likely to increase the heart rate through abnormal sympathetic activity, and the effects of BBG reducing the heart rate may be associated with interrupting this process. Considering that BBG may inhibit other P2X receptors, BBG decreasing the heart rate may be an integrative result of suppression of multiple P2X receptors.

Although ample experimental evidence shows that pharmacological inhibition of P2X7 has therapeutic effects on cardiovascular disease (34), it cannot produce the expected results in clinical trials, and complex backgrounds of disease play a role. For example, diabetes causes the heart to resist many protective measures. In this study, it was noteworthy that both 2 wk of BBG injection before MI/R and acutely administered A438079 at the time of MI/R injury were sufficient to produce less inflammation as well as reduce myocardial infarct area, improve cardiac function, and restrain apoptosis in diabetic mice. Thus, these results reinforced that targeting P2X7 may still protect against myocardial ischemic disease in patients with diabetes.

The present study has some limitations. First, the effects of P2X7 on MI/R injury have been investigated previously. Considering the complexity of the inherent immune system in diabetes, the purpose of this study was to further determine whether P2X7 plays a role in diabetes-aggravated MI/R injury based on previous studies. Second, we validated the role of P2X7 in HFD/STZ-induced diabetes mice, and the condition of P2X7 in other diabetes models remains to be explored. Finally, due to the problem of specificity in agonists and inhibitors, we will generate P2X7 conditional knockout mice for additional studies.

In conclusion, the present findings demonstrated that MI/R-associated cardiac injury differs between normal and diabetic hearts. P2X7 is a critical trigger in vulnerability to MI/R injury under diabetes. Targeting P2X7 may be a novel strategy for attenuating diabetes-induced cardiovascular injury.

Acknowledgments

We thank the Translational Medicine Research Central of Zhujiang Hospital of Southern Medical University for technical assistance.

Disclosures

The authors have no financial conflicts of interest.

References

1. Antonioli, L., C. Blandizzi, B. Csóka, P. Pacher, and G. Haskó. 2015. Adenosine signalling in diabetes mellitus–pathophysiology and therapeutic considerations. *Nat. Rev. Endocrinol.* 11: 228–241.
2. Kleinbongard, P., H. E. Bøtker, M. Ovize, D. J. Hausenloy, and G. Heusch. 2020. Co-morbidities and co-medications as confounders of cardioprotection—does it matter in the clinical setting? *Br. J. Pharmacol.* 177: 5252–5269.
3. Zhang, X. J., X. Liu, M. Hu, G. J. Zhao, D. Sun, X. Cheng, H. Xiang, Y. P. Huang, R. F. Tian, L. J. Shen, et al. 2021. Pharmacological inhibition of arachidonate 12-lipoxygenase ameliorates myocardial ischemia-reperfusion injury in multiple species. *Cell Metab.* 33: 2059–2075.e10.
4. Lejay, A., F. Fang, R. John, J. A. Van, M. Barr, F. Thaveau, N. Chakfe, B. Geny, and J. W. Scholey. 2016. Ischemia reperfusion injury, ischemic conditioning and diabetes mellitus. *J. Mol. Cell. Cardiol.* 91: 11–22.
5. Di Virgilio, F., D. Dal Ben, A. C. Sarti, A. L. Giuliani, and S. Falzoni. 2017. The P2X7 receptor in infection and inflammation. *Immunity* 47: 15–31.
6. De Marchi, E., E. Orioli, A. Pegoraro, S. Sangaletti, P. Portararo, A. Curti, M. P. Colombo, F. Di Virgilio, and E. Adinolfi. 2019. The P2X7 receptor modulates immune cells infiltration, ectonucleotidases expression and extracellular ATP levels in the tumor microenvironment. *Oncogene* 38: 3636–3650.
7. Burnstock, G. 2017. Purinergic signaling in the cardiovascular system. *Circ. Res.* 120: 207–228.
8. Menzies, R. I., J. W. R. Booth, J. J. Mullins, M. A. Bailey, F. W. K. Tam, J. T. Norman, and R. J. Unwin. 2017. Hyperglycemia-induced renal P2X7 receptor activation enhances diabetes-related injury. *EBioMedicine* 19: 73–83.
9. Portillo, J. C., Y. Lopez Corcino, Y. Miao, J. Tang, N. Sheibani, T. S. Kern, G. R. Dubyak, and C. S. Subauste. 2017. CD40 in retinal müller cells induces P2X7-dependent cytokine expression in macrophages/microglia in diabetic mice and development of early experimental diabetic retinopathy. *Diabetes* 66: 483–493.
10. Liu, W., Q. Ao, Q. Guo, W. He, L. Peng, J. Jiang, and X. Hu. 2017. miR-9 mediates CALHM1-activated ATP-P2X7R signal in painful diabetic neuropathy rats. *Mol. Neurobiol.* 54: 922–929.
11. Cheng, Y., X. Yu, J. Zhang, Y. Chang, M. Xue, X. Li, Y. Lu, T. Li, Z. Meng, L. Su, et al. 2019. Pancreatic kallikrein protects against diabetic retinopathy in KK Cg-A^{y}/J and high-fat diet/streptozotocin-induced mouse models of type 2 diabetes. *Diabetologia* 62: 1074–1086.
12. Leach, J. P., T. Heallen, M. Zhang, M. Rahmani, Y. Morikawa, M. C. Hill, A. Segura, J. T. Willerson, and J. F. Martin. 2017. Hippo pathway deficiency reverses systolic heart failure after infarction. *Nature* 550: 260–264.
13. Zhao, J., H. Wang, C. Dai, H. Wang, H. Zhang, Y. Huang, S. Wang, F. Gaskin, N. Yang, and S. M. Fu. 2013. P2X7 blockade attenuates murine lupus nephritis by inhibiting activation of the NLRP3/ASC/caspase 1 pathway. *Arthritis Rheum.* 65: 3176–3185.
14. Deng, H., Y. Zhang, G. G. Li, H. H. Yu, S. Bai, G. Y. Guo, W. L. Guo, Y. Ma, J. H. Wang, N. Liu, et al. 2021. P2X7 receptor activation aggravates NADPH oxidase 2-induced oxidative stress after intracerebral hemorrhage. *Neural Regen. Res.* 16: 1582–1591.
15. Qian, Y., C. Qian, K. Xie, Q. Fan, Y. Yan, R. Lu, L. Wang, M. Zhang, Q. Wang, S. Mou, et al. 2021. P2X7 receptor signaling promotes inflammation in renal parenchymal cells suffering from ischemia-reperfusion injury. *Cell Death Dis.* 12: 132.
16. Xu, J., X. M. Chen, B. J. Zheng, and X. R. Wang. 2016. Electroacupuncture relieves nerve injury-induced pain hypersensitivity via the inhibition of spinal P2X7 receptor-positive microglia. *Anesth. Analg.* 122: 882–892.
17. Kavanagh, D. P. J., A. B. Lokman, G. Neag, A. Colley, and N. Kalia. 2019. Imaging the injured beating heart intravitally and the vasculoprotection afforded by haematopoietic stem cells. *Cardiovasc. Res.* 115: 1918–1932.
18. Donath, M. Y., and S. E. Shoelson. 2011. Type 2 diabetes as an inflammatory disease. *Nat. Rev. Immunol.* 11: 98–107.
19. Sharif, S., Y. Van der Graaf, M. J. Cramer, L. J. Kapelle, G. J. de Borst, F. L. J. Visseren, and J. Westerink; SMART study group. 2021. Low-grade inflammation as a risk factor for cardiovascular events and all-cause mortality in patients with type 2 diabetes. *Cardiovasc. Diabetol.* 20: 220.
20. Schiattarella, G. G., D. Rodolico, and J. A. Hill. 2021. Metabolic inflammation in heart failure with preserved ejection fraction. *Cardiovasc. Res.* 117: 423–434.
21. Donath, M. Y., C. A. Dinarello, and T. Mandrup-Poulsen. 2019. Targeting innate immune mediators in type 1 and type 2 diabetes. *Nat. Rev. Immunol.* 19: 734–746.
22. Ridker, P. M., B. M. Everett, T. Thuren, J. G. MacFadyen, W. H. Chang, C. Ballantyne, F. Fonseca, J. Nicolau, W. Koenig, S. D. Anker, et al.; CANTOS Trial Group. 2017. Antiinflammatory therapy with canakinumab for atherosclerotic disease. *N. Engl. J. Med.* 377: 1119–1131.
23. Genetzakis, E., J. Gilchrist, M. Kassiou, and G. A. Figtree. 2022. Development and clinical translation of P2X7 receptor antagonists: a potential therapeutic target in coronary artery disease? *Pharmacol. Ther.* 237: 108228.
24. Lafuse, W. P., D. J. Wozniak, and M. V. S. Rajaram. 2020. Role of cardiac macrophages on cardiac inflammation, fibrosis and tissue repair. *Cells* 10: 51.
25. Knapp, M., X. Tu, and R. Wu. 2019. Vascular endothelial dysfunction, a major mediator in diabetic cardiomyopathy. *Acta Pharmacol. Sin.* 40: 1–8.
26. Pellegrini, C., A. Martelli, L. Antonioli, M. Fornai, C. Blandizzi, and V. Calderone. 2021. NLRP3 inflammasome in cardiovascular diseases: pathophysiological and pharmacological implications. *Med. Res. Rev.* 41: 1890–1926.
27. Toldo, S., and A. Abbate. 2018. The NLRP3 inflammasome in acute myocardial infarction. *Nat. Rev. Cardiol.* 15: 203–214.
28. Garcia-Jacobo, R. E., L. S. Bergamin, V. Vultaggio-Poma, M. L. Thorstenberg, M. Tarantini, M. H. García-Hernández, and F. Di Virgilio. 2022. The purinergic landscape of type 2 diabetes mellitus. *Molecules* 27: 1838.
29. McCarthy, A. E., C. Yoshioka, and S. E. Mansoor. 2019. Full-length P2X$_7$ structures reveal how palmitoylation prevents channel desensitization. *Cell* 179: 659–670.e13.

30. Antonioli, L., P. Pacher, E. S. Vizi, and G. Haskó. 2013. CD39 and CD73 in immunity and inflammation. *Trends Mol. Med.* 19: 355–367.
31. Chen, P. S., L. S. Chen, J. M. Cao, B. Sharifi, H. S. Karagueuzian, and M. C. Fishbein. 2001. Sympathetic nerve sprouting, electrical remodeling and the mechanisms of sudden cardiac death. *Cardiovasc. Res.* 50: 409–416.
32. Ong, S. B., S. Hernández-Reséndiz, G. E. Crespo-Avilan, R. T. Mukhametshina, X. Y. Kwek, H. A. Cabrera-Fuentes, and D. J. Hausenloy. 2018. Inflammation following acute myocardial infarction: multiple players, dynamic roles, and novel therapeutic opportunities. *Pharmacol. Ther.* 186: 73–87.
33. Vinik, A. I., T. Erbas, and C. M. Casellini. 2013. Diabetic cardiac autonomic neuropathy, inflammation and cardiovascular disease. *J. Diabetes Investig.* 4: 4–18.
34. Shokoples, B. G., P. Paradis, and E. L. Schiffrin. 2021. P2X7 receptors: an untapped target for the management of cardiovascular disease. *Arterioscler. Thromb. Vasc. Biol.* 41: 186–199.